N_2O isotopocule measurements using laser spectroscopy: analyzer characterization and intercomparison

Stephen J. Harris[1,2,*], Jesper Liisberg[3,*], Longlong Xia[4], Jing Wei[5], Kerstin Zeyer[5], Longfei Yu[5], Matti Barthel[6], Benjamin Wolf[4], Bryce F.J. Kelly[1], Dioni I. Cendón[2], Thomas Blunier[3], Johan Six[6], Joachim Mohn[5]

Supplementary Material

Supplementary Material 1 - IRMS Methodology

IRMS analyses were conducted at ETH Zürich using a gas preparation unit (Trace Gas, Elementar, Manchester, UK) coupled to an IsoPrime100 IRMS (Elementar, Manchester, UK). The gas preparation unit was modified with an additional chemical trap (0.5 in diameter stainless steel), located immediately downstream from the autosampler to pre-condition samples. This pre-trap was filled before each run with new NaOH, $Mg(ClO_4)_2$, and activated carbon in the direction of flow and was designed as a first step to scrub CO_2 and H_2O. After pre-scrubbing, the samples were purged through a second set of chemical traps (NaOH, $Mg(ClO_4)_2$) before cryogenic trapping and focusing in liquid N_2. Before final injection into the IRMS, the purified gas sample was directed through a permeation drier and subsequently separated in a gas chromatograph column (5 Å molecular sieve). The IRMS is equipped with five Faraday cups with *m/z* of 30, 31, 44, 45, 46, measuring $\delta^{15}N^{bulk}$ and $\delta^{18}O$ of N_2O and $\delta^{15}N$ of the NO^+ molecule dissociated from N_2O during ionization in the source. The $^{15}N/^{14}N$ ratio of the NO molecule reflects the α (central) position N of the initial N_2O, thus allowing the measurement of the site-specific isotopic composition of N_2O. During each run three sets of two working standards (~ 3 ppm N_2O mixed in synthetic air) with different isotopic composition ($\delta^{15}N^{\alpha}$ = 0.954 ± 0.123 ‰ and 34.446 ± 0.179 ‰; $\delta^{15}N^{\beta}$ = 2.574 ± 0.086 ‰ and 35.98 ± 0.221 ‰; $\delta^{18}O$ = 39.741 ± 0.051 ‰ and 38.527 ± 0.107 ‰) were included with a batch of 22 samples at the beginning, middle and end of each run. Sample peak ratios are initially reported against a N_2O reference gas peak (100% N_2O, Carbagas, Gümligen, Switzerland) and are subsequently corrected for drift and span using the working standards. Instrument linearity and stability was frequently checked

by injection of 10 reference gas pulses of either varying or identical height respectively, with accepted levels of < 0.03 ‰ nA^{-1}. Since instrument linearity could only be achieved for either N_2O or NO, the instrument was tuned for the former and $\delta^{15}N^{\alpha}$ non-linearity subsequently corrected using sample peak heights by determining non-linearity of $\delta^{15}N^{\alpha}$ with diluted working standards.

Supplementary Material 2 - Experimental setups

Figs. S2-1 to S2-10 depict the setup for the gas matrix, trace gas and two end-member mixing experiments undertaken in this study. Experiments were performed simultaneously for all analyzers, with the exception of the TREX-QCLAS, which requires an extensive measurement protocol to trap and measure N_2O (Ibraim et al., 2018) and thus could not be integrated concurrently with the other analyzers.

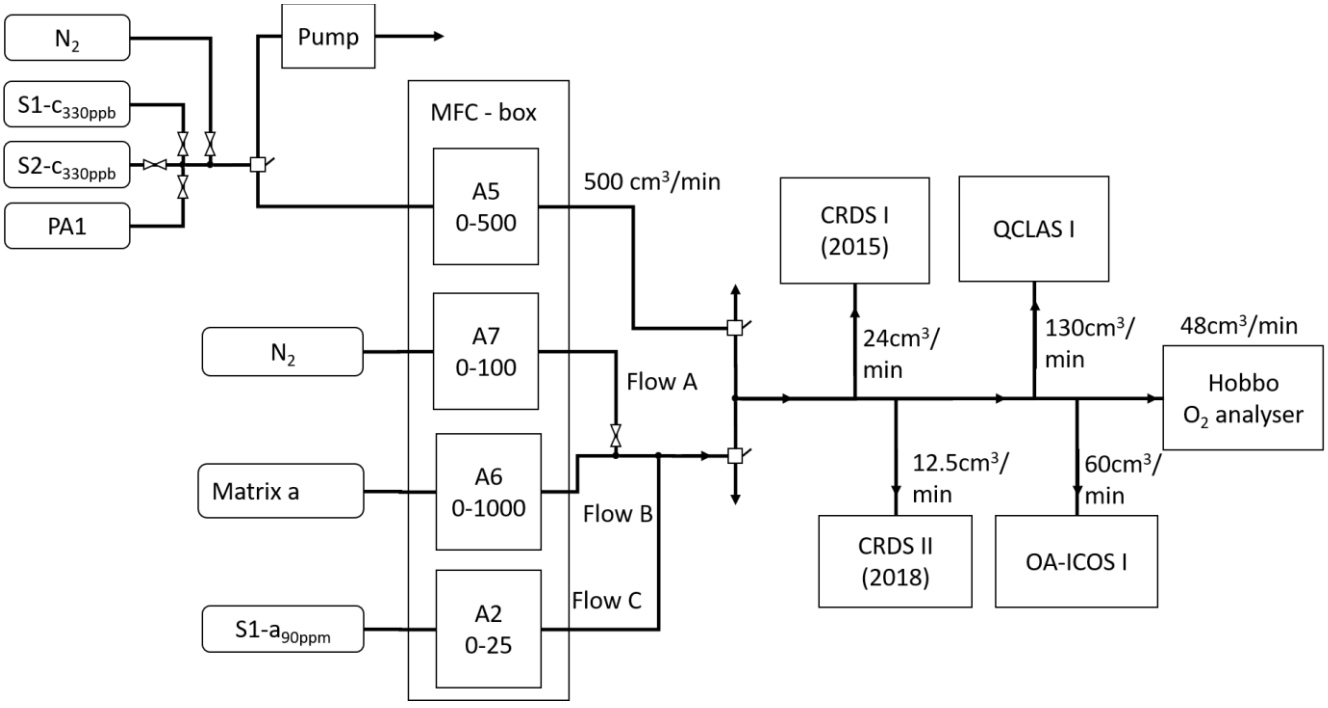

Fig. S2-1. Experimental setup for the O_2 dependence testing performed in Section 2.4.5.

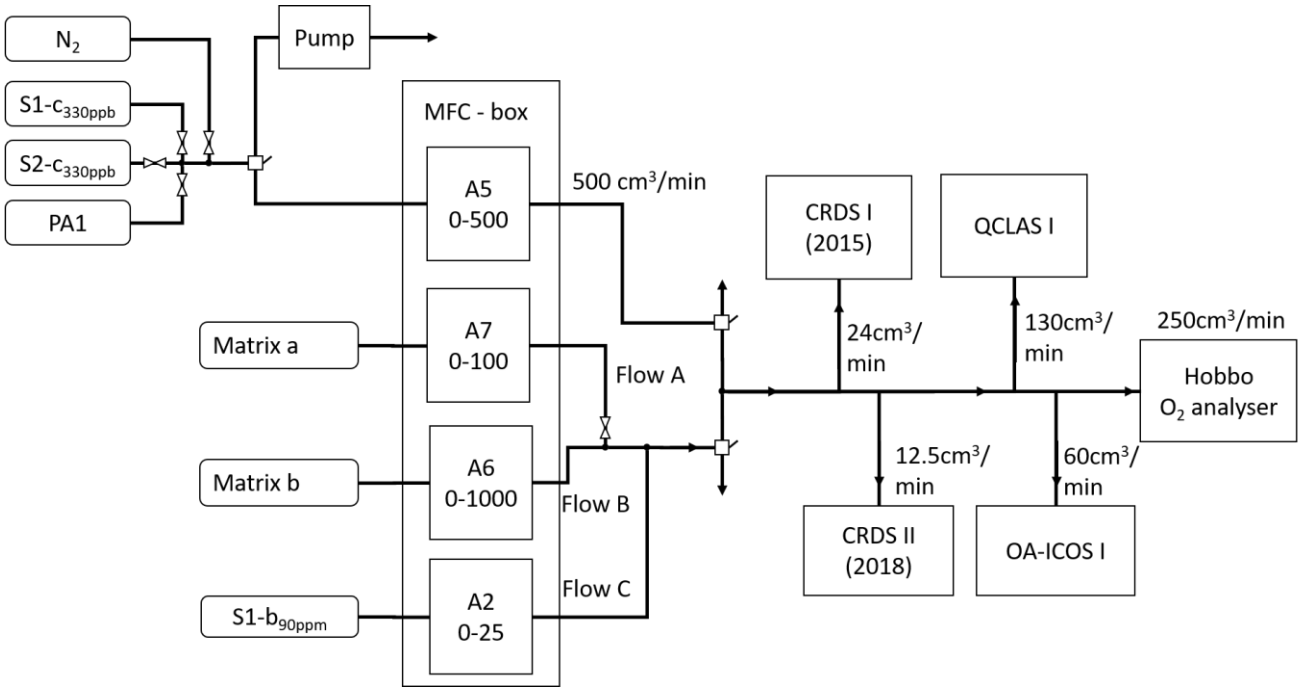

Fig. S2-2. Experimental setup for the Ar dependence testing performed in Section 2.4.5.

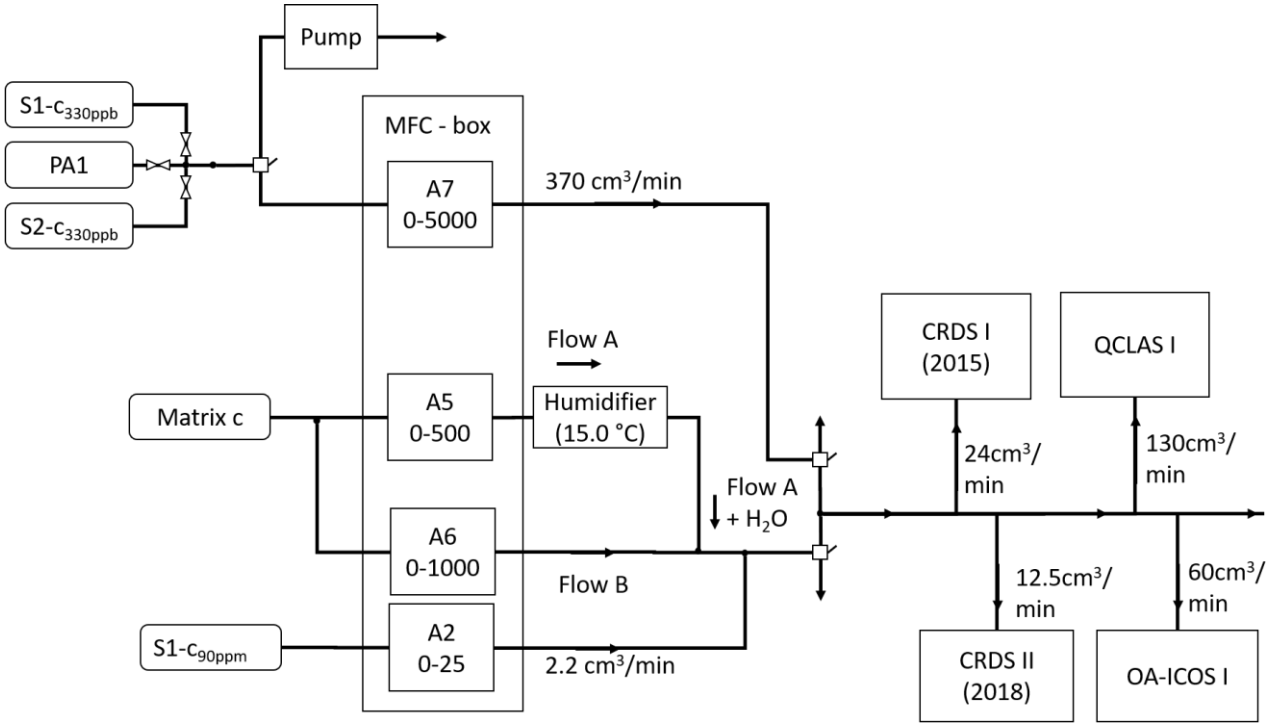

Fig. S2-3. Experimental setup for the H_2O dependence testing performed in Section 2.4.6.

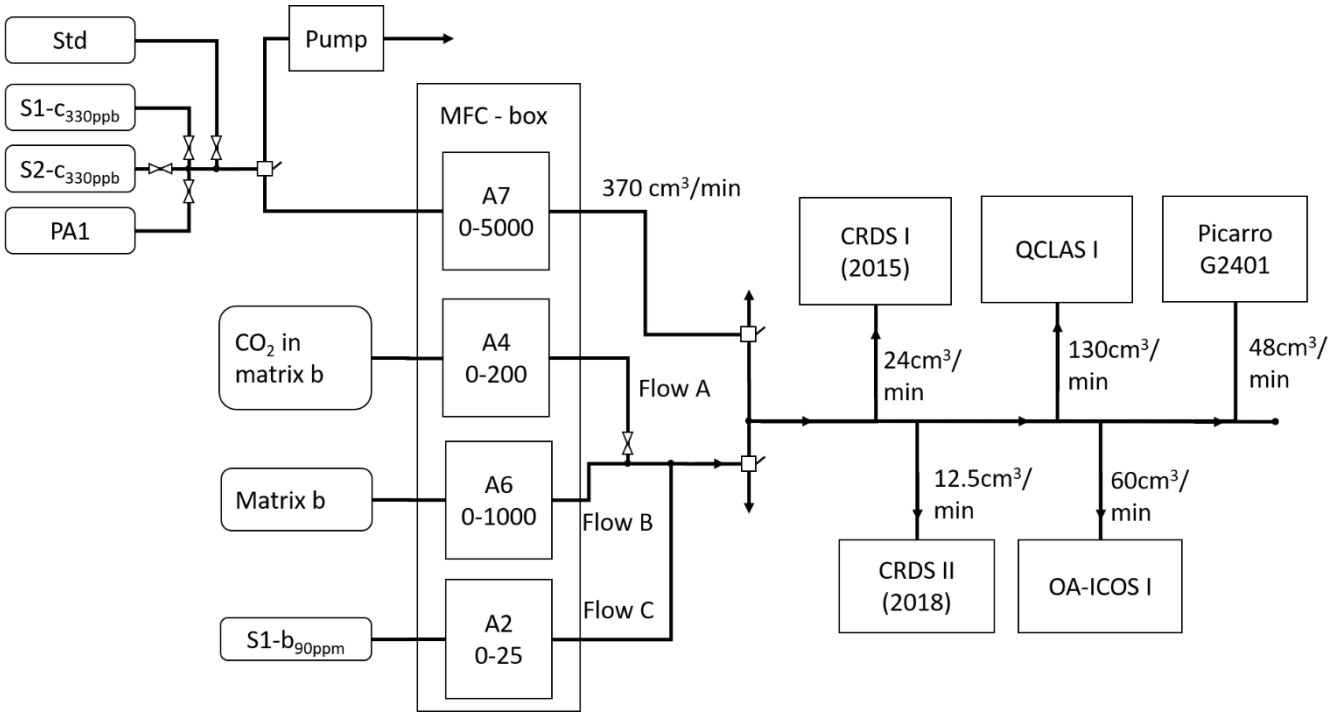

Fig. S2-4. Experimental setup for the CO_2 dependence testing performed in Section 2.4.6.

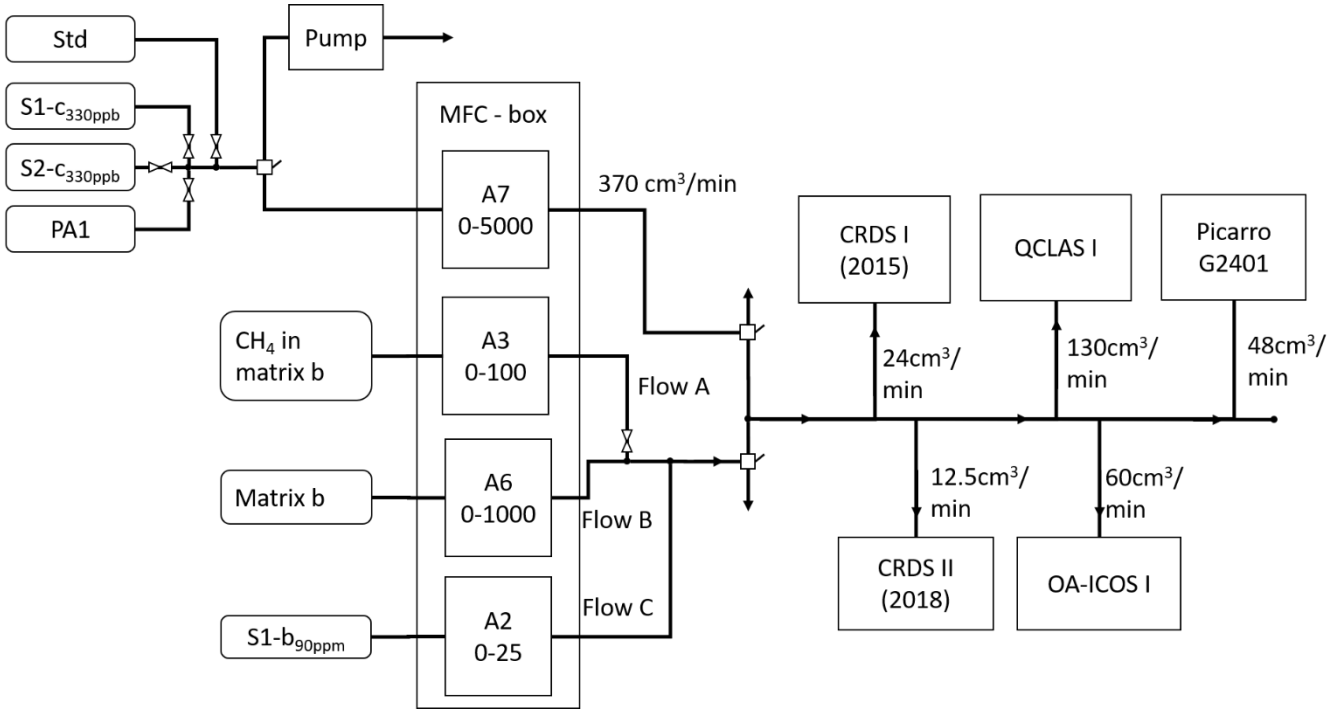

Fig. S2-5. Experimental setup for the CH_4 dependence testing performed in Section 2.4.6.

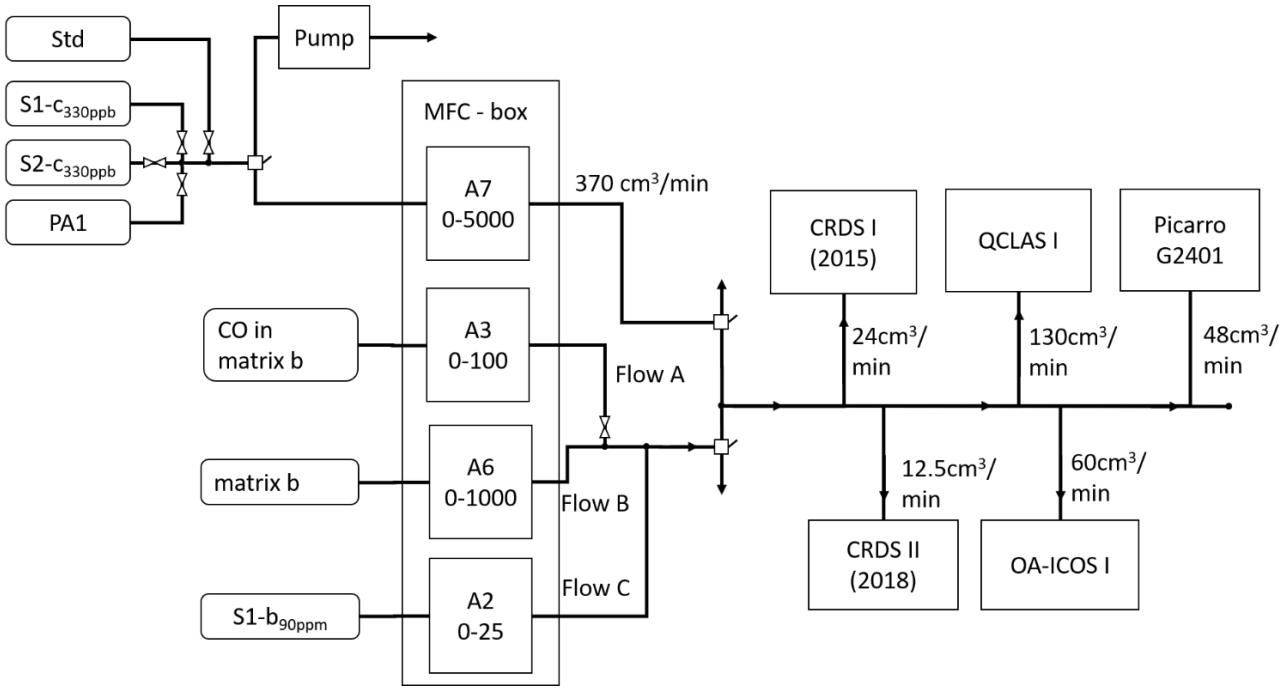

Fig. S2-6. Experimental setup for the CO dependence testing performed in Section 2.4.6.

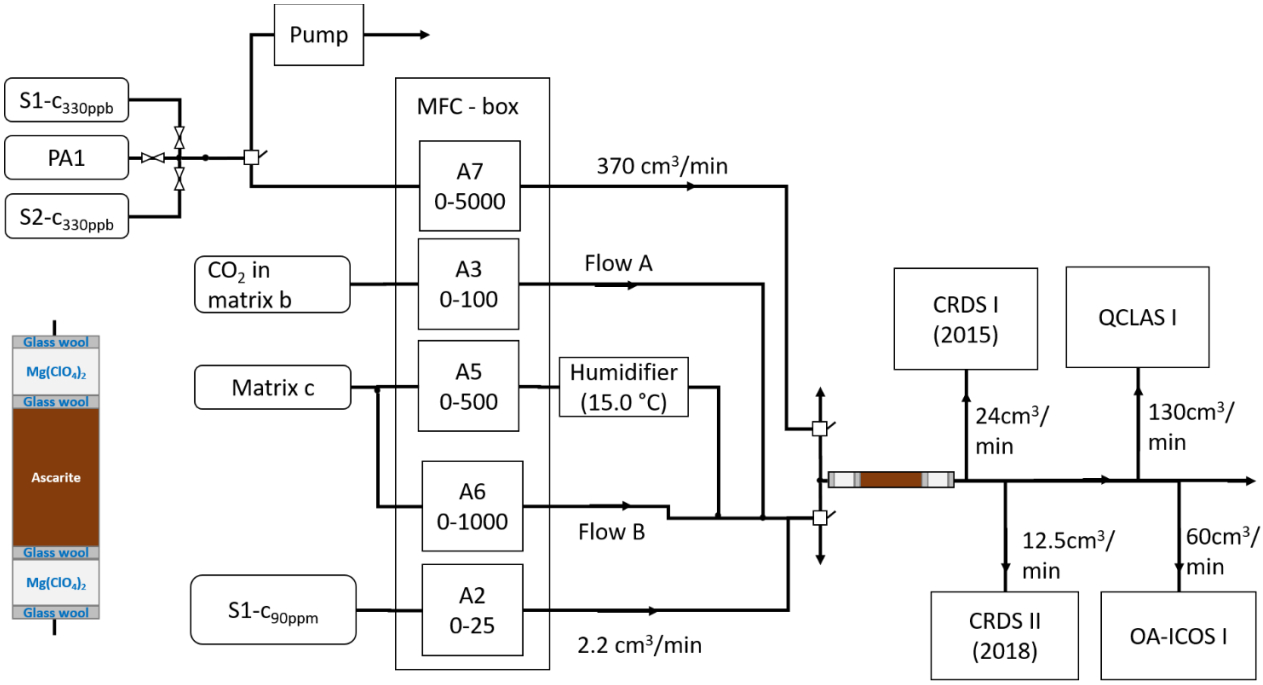

Fig. S2-7. Experimental setup for the Ascarite and Sofnocat trap testing performed in Section 2.4.7.

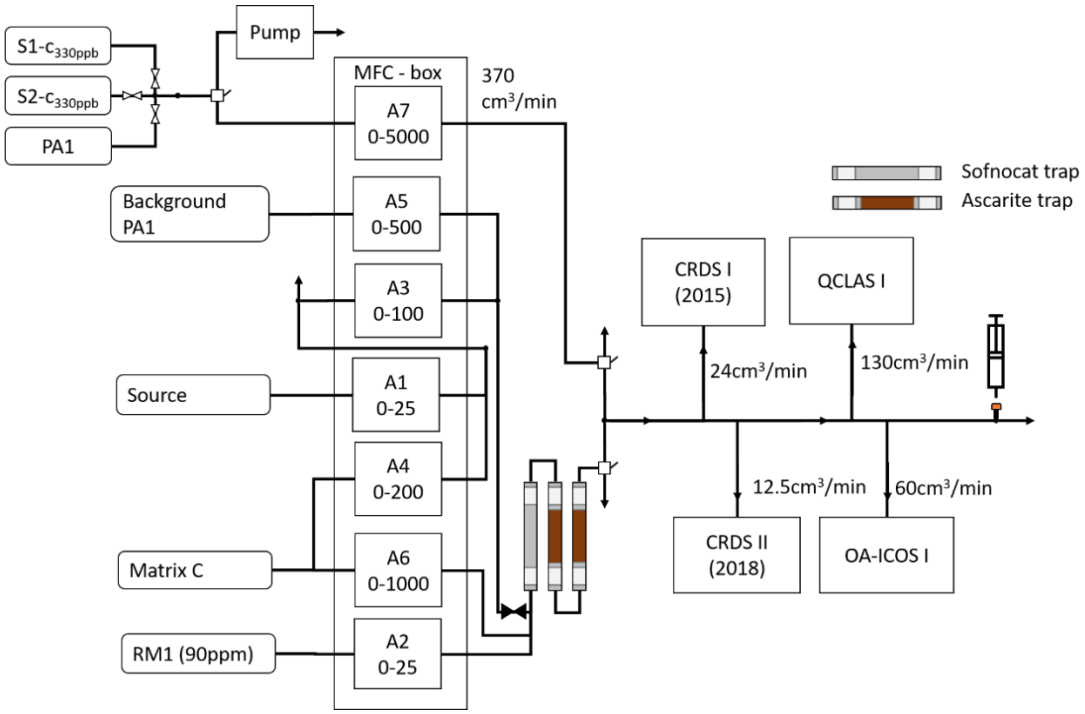

Fig. S2-8. Experimental setup for Experiments 1 and 2 performed in Section 2.4.8.

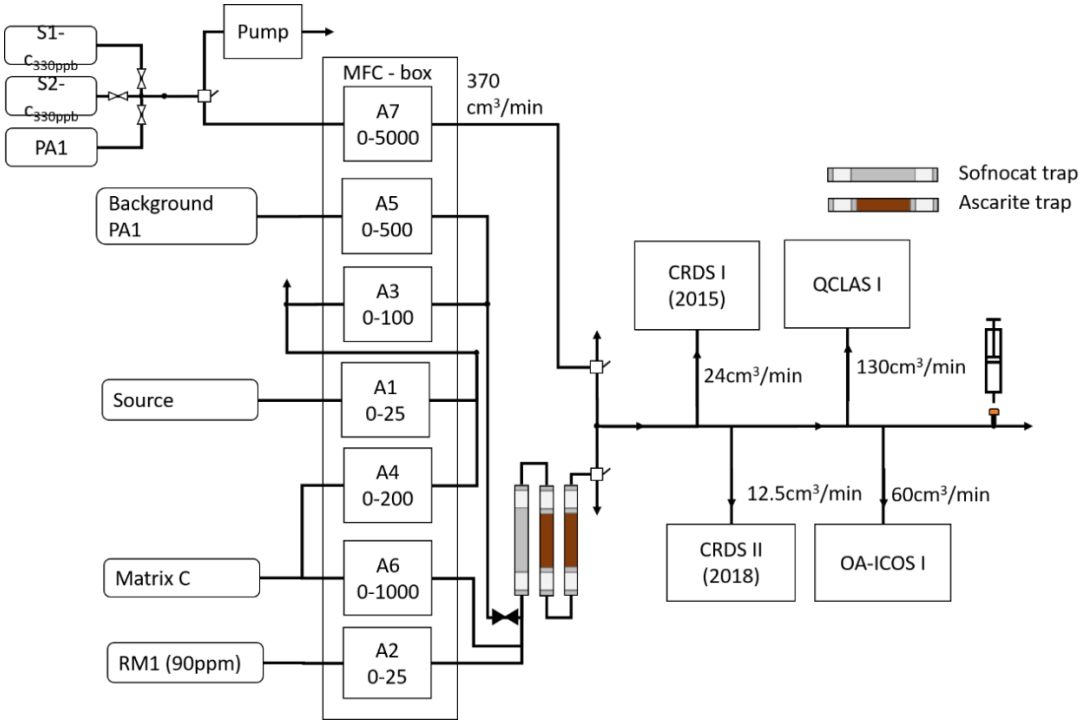

Fig. S2-9. Experimental setup for Experiments 3 and 4 performed in Section 2.4.8.

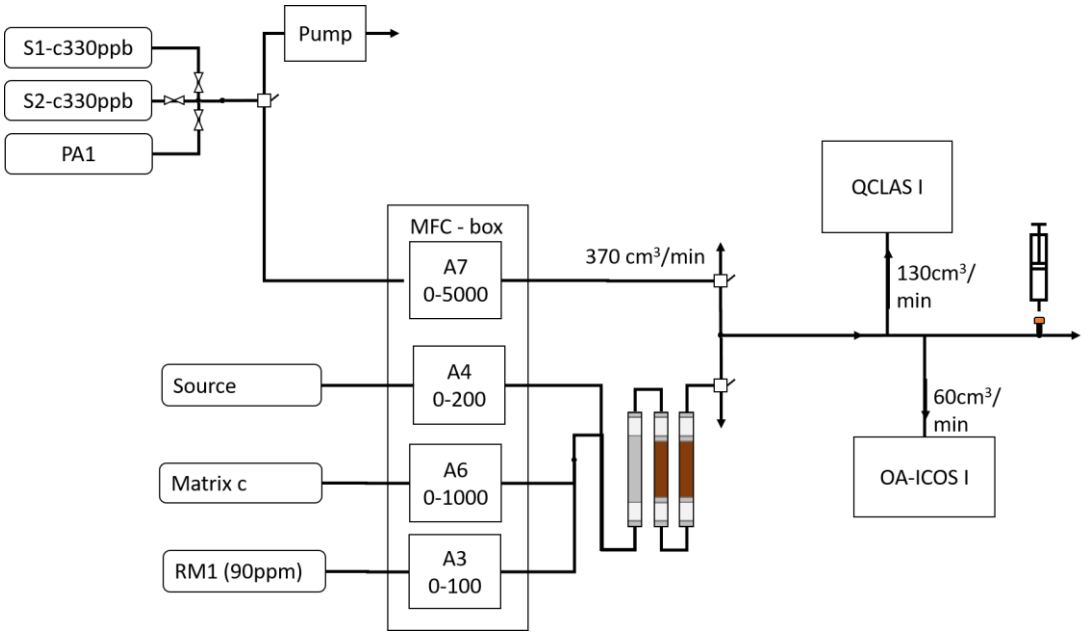

Fig. S2-10. Experimental setup for Experiments 5 and 6 performed in Section 2.4.8.

Supplementary Material 3 – Application of an automatic spectral correction method for QCLAS measurements

The primary cause of the observed excess drift in QCLAS I isotopocule measurements was fluctuating spectral baseline structure. That baseline structure, at an absorbance level of ~5×10^{-5} , was likely due to interference fringes that were enhanced by somewhat dirty absorption cell mirrors (pers. comm. Aerodyne Research Inc.). One way to reduce the effects of excess baseline structure is to employ the instrument operation mode "Automatic Background", wherein a spectrum is recorded while zero-air is injected, and subsequent spectra are divided by the recorded background spectrum. Periodic zero-air injections with refreshed background spectra can reduce the effect of changing baseline structure. Aerodyne recommends that "Automatic Background" be used in measurements with very weak absorptions, such as in the measurements reported in this paper. However, Aerodyne Research Inc. recognizes that frequent backgrounds may not be convenient or practical in all circumstances. Also, instrument operators may not observe a gradual increase in baseline structure over time.

Recently, Aerodyne has been developing a new method of correcting data that is influenced by changing baseline structure. In this new method, injections of zero air and calibrations may be less frequent than would otherwise be necessary. An outline of the correction method provided by Aerodyne Research Inc. is as follows. Mixing ratio (MR) and spectral data are grouped according to type: background gas, calibration gas (Cal), and air sample measurements. Averages for the MR's and spectra for the groups are subtracted. An aggregate subtracted spectrum array is smoothed to the absorption linewidth. A principal component analysis [PCA] is performed, so that spectral fluctuations are represented as a sum of vectors, $V_i(x)$, times amplitude histories, $A_i(t)$. For the "Cal" segments, we fit the recorded MR's with a sub-set of $\{A_i(t)\}$. If the specific linear combination of $\{A_i(t)\}$ from the MR fit well-represent the "Cal" segments, we apply that linear combination of $\{A_i(t)\}$ to the full measured data-set to determine MR adjustments.

In the Allan variance experiments performed on QCLAS I in this study (Sect. 3.1), the instruments were continuously sampling from a tank, so fictive hourly calibration periods (5 m duration) were created and used to generate mixing-ratio corrections. This method is computationally rapid, as ~8 hr of MR data can be adjusted in seconds. A summary of the corrected data is provided in Table S3-1. This new method is not yet published or broadly verified, but Aerodyne Research Inc. intends, after further validation, to share the methodology with the measurement community.

Table S3-1. Summary of the corrected QCLAS I Allan variance data acquired in Sect. 3.1. 1σ data refers to Allan deviation (square root of Allan variance).

	N_2O [ppb]			$\delta^{15}N^{\alpha}$ [‰]			$\delta^{15}N^{\beta}$ [‰]		
N_2O [ppb]	1σ (1s)	1σ (300s)	1σ (600s)	1σ (1s)	1σ (300s)	1σ (600s)	1σ (1s)	1σ (300s)	1σ (600s)
326.5	0.062	0.021	0.024	1.2	0.39	0.37	1.7	0.42	0.55
1000	0.165	0.14	0.10	1.4	0.19	0.23	1.4	0.20	0.22
10000	2.9	0.46	0.38	0.33	0.027	0.029	0.25	0.024	0.028

Supplementary Material 4 – Short-term repeatability

To test the short-term repeatability of the instruments, sample gas at different at different [N_2O]: ambient (PA1), 1 ppm , 10 ppm N_2O was repeatedly analyzed 10 times for 15 min, intercepted by dry ambient air for 5 min. Gas mixtures with 1 and 10 ppm N_2O were prepared by dynamically diluting S1-c_{90ppm} with matrix gas c.. All data were corrected for drift using a linear interpolation of two bracketing anchor gas measurements (cf. Lebegue et al., 2016).

In Table S4-1 and S4-2 the short–term repeatability is expressed as standard deviation (1σ) of 10 repeated measurements using averaging times of 300 s and 600 s, respectively. At ~327 ppb N_2O, the best repeatability for δ values was achieved by TREX–QCLAS I, with around 0.3 ‰ for $\delta^{15}N^{\alpha}$, $\delta^{15}N^{\beta}$, and $\delta^{18}O$ at 300 s averaging. The CRDS analyzers showed a similar repeatability level of 0.25–0.40 ‰ for all δ values, at 600 s averaging, somewhat worse 0.35–0.6 ‰ at 300 s, but without the requirement for preconcentration. OA-ICOS I achieved a repeatability of 0.75 ‰ (1.1 ‰) for $\delta^{15}N^{\alpha}$ and $\delta^{15}N^{\beta}$, and 1.3 ‰ (2.4‰) for $\delta^{18}O$ at 600 s (300 s) averaging. QCLAS analyzers without preconcentration (QCLAS I) showed poor repeatability for δ values regardless of averaging time, in-line with results acquired in Sect. 3.1. In contrast to δ values, the best [N_2O] repeatability was achieved by both the OA-ICOS I and QCLAS I (0.02 ppb), while the repeatability was worst for TREX–QCLAS I (0.48 ppb), due to the multiple parameters involved in [N_2O] analysis.

At 1 ppm N_2O, the repeatability of δ-measurements improved for all instruments, with the exception of CRDS I, compared to ~327 ppb N_2O. CRDS II achieved the best repeatability of 0.15 – 0.24 ‰ (0.20 – 0.26 ‰) for δ values at 600 s (300 s) averaging, while the repeatability for CRDS I did not profit from an increase in [N_2O] but degraded to 0.39 – 0.49 ‰ (0.65 – 0.91 ‰). OA-ICOS I achieved a repeatability of 0.28–0.37 ‰ (0.21–0.27 ‰) for $\delta^{15}N^{\alpha}$ and $\delta^{15}N^{\beta}$ and 0.69 ‰ (0.54 ‰) for $\delta^{18}O$ at 300 s (600 s) averaging. QCLAS I showed again the weakest repeatability for δ values of 2–7 ‰, irrespective of the averaging time. Again the best repeatability for [N_2O] was achieved by OA-ICOS I and QCLAS I but worsened for all instruments compared to ~327 ppb N_2O.

At 10 ppm N_2O, δ-measurement repeatability improved further compared to both near-atmospheric and 1 ppm measurements. The best repeatability was demonstrated by OA-ICOS I with 0.09‰, 0.16‰ and 0.20‰ at 300 s averaging, and 0.06‰, 0.13‰ and 16‰ at 600 s averaging for $\delta^{15}N^{\alpha}$, $\delta^{15}N^{\beta}$ and $\delta^{18}O$, respectively. The repeatability of QCLAS I was also largely improved to 0.3–0.45 ‰ for $\delta^{15}N^{\alpha}$ and $\delta^{15}N^{\beta}$. In contrast, QCLAS I achieved the best [N_2O] repeatability of 1.05 ppb (1.45 ppb) at 600 s (300 s) averaging.

Table S4-1. Repeatability acquired for [N_2O], $\delta^{15}N^{\alpha}$, $\delta^{15}N^{\beta}$ and $\delta^{18}O$ as standard deviation (1σ) for 10 repeated measurements at 300 s averaging time. Measurements were made at 326.5 ppb (PA1), 1000 ppb and 10000 ppb N_2O.

Instrument	*n*	1σ N_2O [ppb]	N_2O range [ppb]	1σ $\delta^{15}N^{\alpha}$ [‰]	$\delta^{15}N^{\alpha}$ range [‰]	1σ $\delta^{15}N^{\beta}$ [‰]	$\delta^{15}N^{\beta}$ range [‰]	1σ $\delta^{18}O$ [‰]	$\delta^{18}O$ range [‰]
326.5 ppb N_2O									
CRDS I	10	0.17	0.50	0.48	1.82	0.38	1.07	0.59	2.03
CRDS II	10	0.05	0.13	0.58	1.64	0.37	1.14	0.35	0.94
OA-ICOS I	10	0.02	0.06	1.12	3.32	1.14	3.26	2.40	7.06
QCLAS I	10	0.02	0.05	6.60	19.19	9.84	31.35	-	-
TREX-QCLAS I	10	0.48	1.36	0.27	0.68	0.31	0.97	0.29	0.73
1000 ppb N_2O									
CRDS I	10	0.87	2.78	0.75	2.37	0.91	2.82	0.65	1.95
CRDS II	10	0.45	1.15	0.20	0.70	0.26	0.91	0.23	0.61
OA-ICOS I	10	0.24	0.88	0.37	1.40	0.28	0.83	0.69	2.28
QCLAS I	10	0.31	0.87	2.38	7.47	6.62	16.75	-	-
10000 ppb N_2O									
OA-ICOS I	10	2.13	6.65	0.09	0.26	0.16	0.49	0.20	0.64
QCLAS I	10	1.45	4.77	0.28	0.99	0.43	1.54	-	-

Table S4-2. Repeatability acquired for [N_2O], $\delta^{15}N^{\alpha}$, $\delta^{15}N^{\beta}$ and $\delta^{18}O$ as standard deviation (1σ) for 10 repeated measurements at 600s averaging time. Measurements were made at 326.5 ppb (PA1), 1000 ppb and 10000 ppb N_2O.

Instrument	*n*	1σ N_2O [ppb]	N_2O range [ppb]	1σ $\delta^{15}N^{\alpha}$ [‰]	$\delta^{15}N^{\alpha}$ range [‰]	1σ $\delta^{15}N^{\beta}$ [‰]	$\delta^{15}N^{\beta}$ range [‰]	1σ $\delta^{18}O$ [‰]	$\delta^{18}O$ range [‰]
326.5 ppb N_2O									
CRDS I	10	0.17	0.48	0.39	1.12	0.23	0.84	0.37	1.43
CRDS II	10	0.05	0.13	0.34	1.04	0.29	1.04	0.30	1.07
OA-ICOS I	10	0.01	0.04	0.77	2.33	0.75	2.05	1.29	3.45
QCLAS I	10	0.02	0.06	6.99	17.63	11.66	32.97	-	-
1000 ppb N_2O									
CRDS I	10	0.66	2.05	0.49	1.72	0.48	1.47	0.39	1.15
CRDS II	10	0.39	1.15	0.24	0.70	0.15	0.46	0.16	0.50
OA-ICOS I	10	0.23	0.69	0.27	0.88	0.21	0.61	0.54	1.84
QCLAS I	10	0.21	0.62	2.21	7.19	6.34	16.30	-	-
10000 ppb N_2O									
OA-ICOS I	10	1.61	4.79	$6.3 \cdot 10^{-2}$	0.17	0.13	0.47	0.16	0.56
QCLAS I	10	1.05	3.09	0.28	0.89	0.46	1.64	-	-

Supplementary Material 5 – Scaling of the signal-to-noise ratio

Expanding on the N_2O mole fraction dependence testing performed in Sect. 2.4.4, we plotted the uncertainty (1σ) of the single 5 min-averaged measurements performed across the three days of mole fraction dependence experimentation acquired by each analyzer, as shown in Fig. S5-1. Because the 5-min averaged data is acquired at the frequency rates as outlined in Table 1, individual points in Fig. S5-1 broadly correspond to the initial *starting point* of each Allan deviation plot (1s for OA-ICOS I, QCLAS I, II and III; 3.41s for CRDS I; 2.54s for CRDS II) for each analyzer measuring at a given N_2O mole fraction. Fig. S5-1 is therefore a useful guide for determining the theoretical optimum measurement precision range for each analyzer. The behavior of this δ-measurement uncertainty as a function of N_2O mole fraction is also of great interest, as this will have important implications for situations where

measurements cannot be repeated in order to increase certainty in the measurement (e.g. low sample volume or soil flux chamber measurements). For δ measurements, the greatest precision is likely to achieved by OA-ICOS I between ~6000–20000 ppb N_2O, CRDS I and II between ~500–1000 ppb N_2O, and QCLAS I between ~30000–90000 ppb.

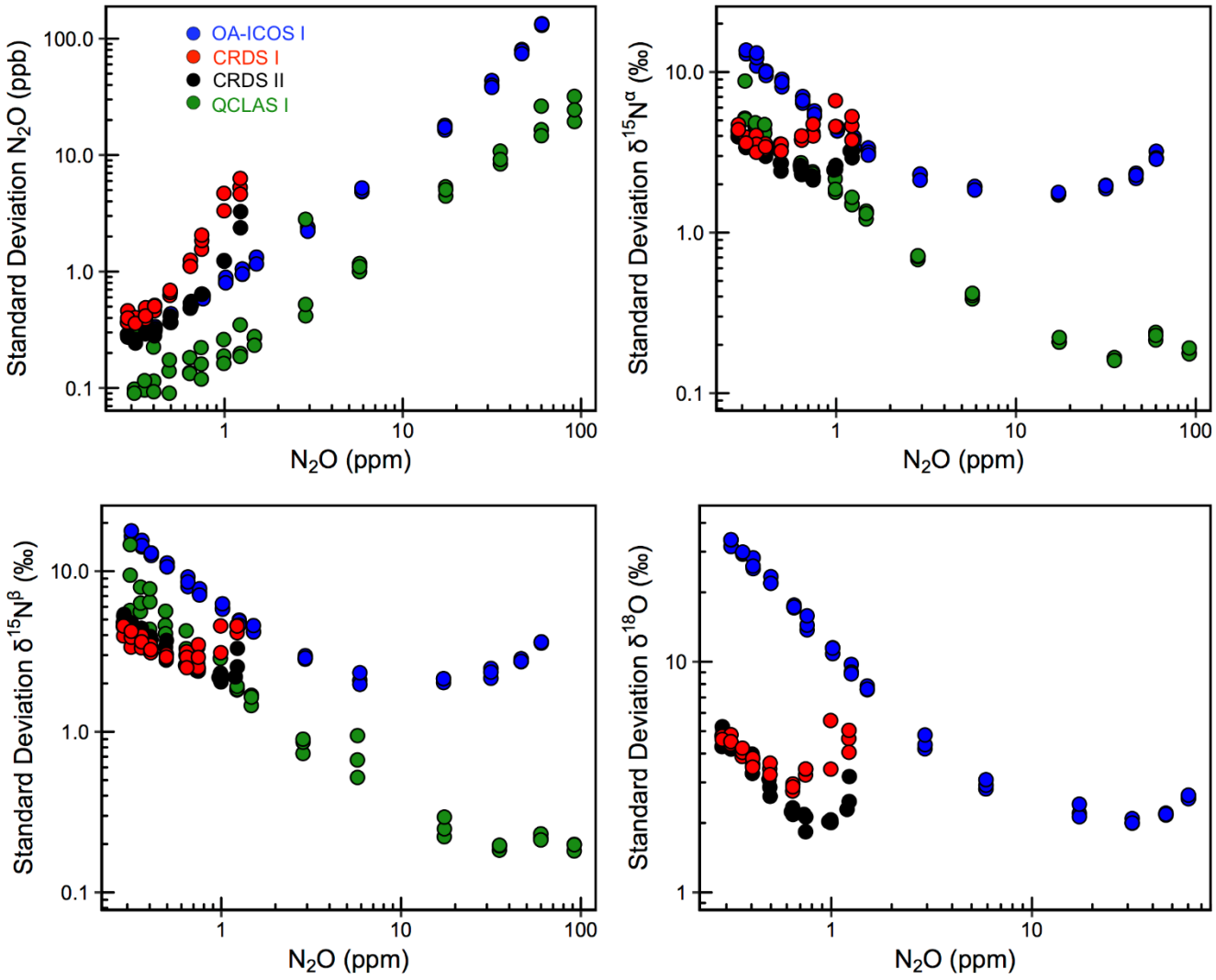

Fig. S5-1. Scaling of single measurement standard deviation (1σ; 300 second averaging time) as a function of N_2O mole fraction for the OA-ICOS I (blue), CRDS I (red), CRDS II (black) and QCLAS I (green). Data was acquired during the mole fraction dependence testing depicted in Fig. 5.

Supplementary Material 6 – Continuity of gas matrix and trace gas corrections at higher N_2O mole fractions

Gas matrix (O_2) and trace gas (CO_2, CH_4 and CO) experiments conducted at 660 and 990 ppb N_2O showed that the interference effects on N_2O mole fraction and delta values is also dependent on N_2O mole fraction. Figs. S6-1 to S6-4 show all data (330, 660 and 990 ppb N_2O) acquired during O_2, CO_2, CH_4 and CO dependence testing, and shows data corrected using Eqs. (7-8) for O_2 and Eq. (9) for CO_2, CH_4 and CO. Corrected data is provided if the linear regression conducted at 330 ppb N_2O for the interference effect was statistically significant at $p < 0.05$. The similarity between the CH_4 and CO dependencies for N_2O mole fraction measurements across all instruments suggests that the apparent effects may be due to the dynamic dilution process, rather than a discrete spectral interference effect. Therefore, data has not been corrected for these effects. Correction using Eqs. (7-8) and Eqs. (11-12) removes the matrix and trace gas effects to the extent that corrected measurements are typically within the uncertainty bounds of the anchor. The O_2 constants A and B, and a, b and c estimated for each analyzer are provided in Table S6-1, while the approximated trace gas constant values of A_x, B_x, a_x and b_x for each analyzer are provided in Table S6-2.

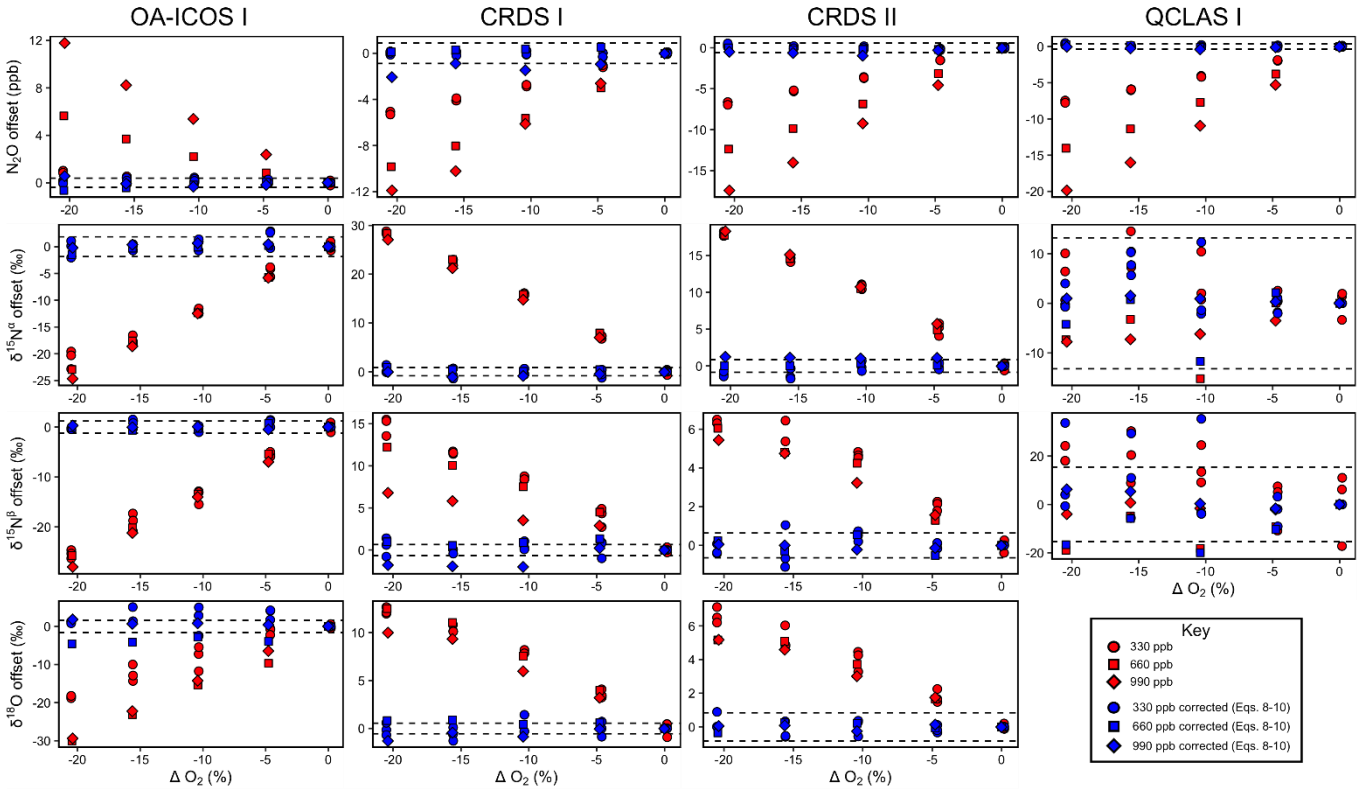

Fig. S6-1. Dependency of the measured [N_2O], $\delta^{15}N^{\alpha}$, $\delta^{15}N^{\beta}$ and $\delta^{18}O$ values on changing O_2 content (%) for OA-ICOS I, CRDS I, CRDS II, and QCLAS I. Non-corrected data is shown in red for various N_2O mole fraction testing (circle = 330 ppb; square = 660 ppb; diamond = 990 ppb). Corrected data using Eqs. (7-8) is shown in blue. The standard deviation of the Anchor gas (±1σ) is indicated by dashed lines.

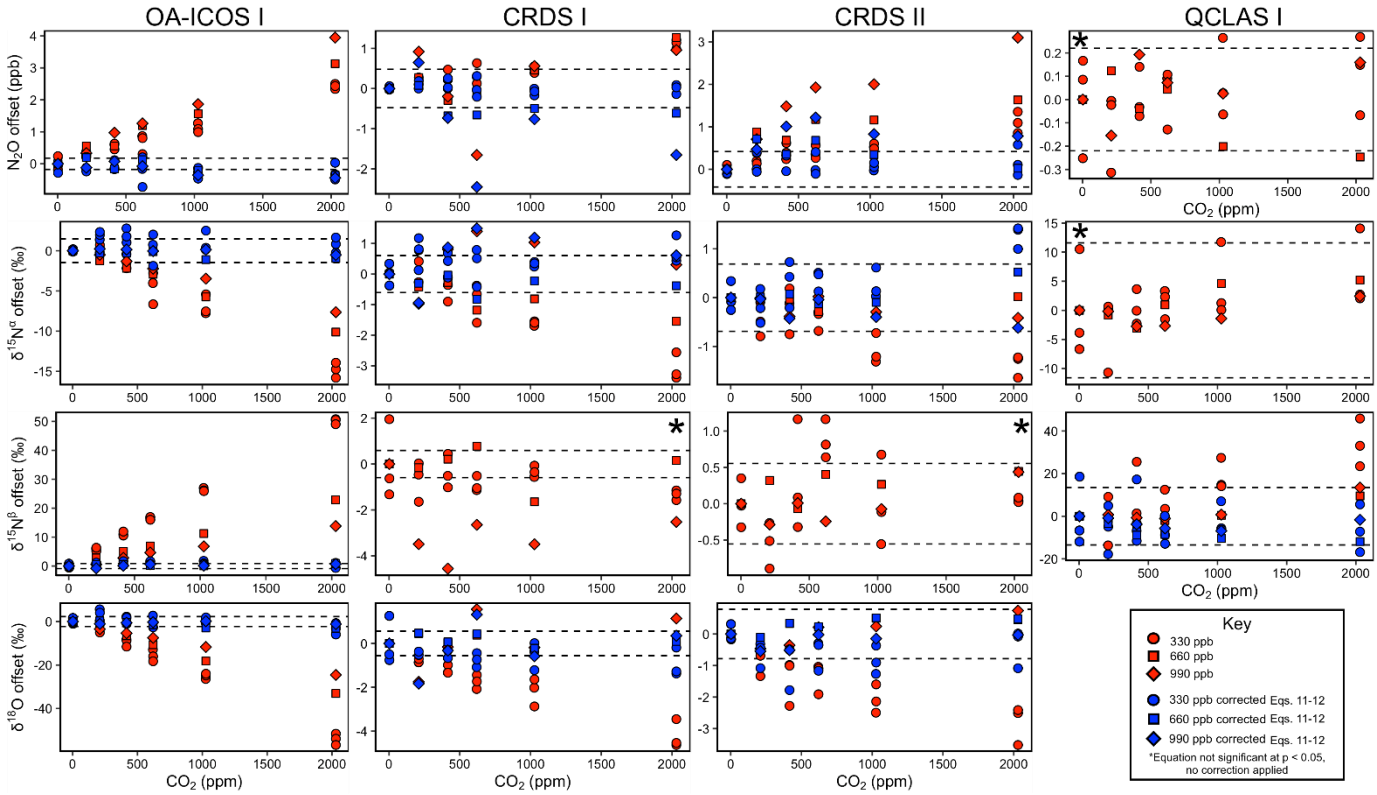

Fig. S6-2. Dependency of the measured [N_2O], $\delta^{15}N^{\alpha}$, $\delta^{15}N^{\beta}$ and $\delta^{18}O$ values on CO_2 (ppm) for OA-ICOS I, CRDS I, CRDS II, and QCLAS I. Non-corrected data is shown in red for various N_2O mole fraction testing (circle = 330 ppb; square = 660 ppb; diamond = 990 ppb). Corrected data using Eqs. (11-12) is shown in blue. The standard deviation of the Anchor gas (±1σ) is indicated by dashed lines.

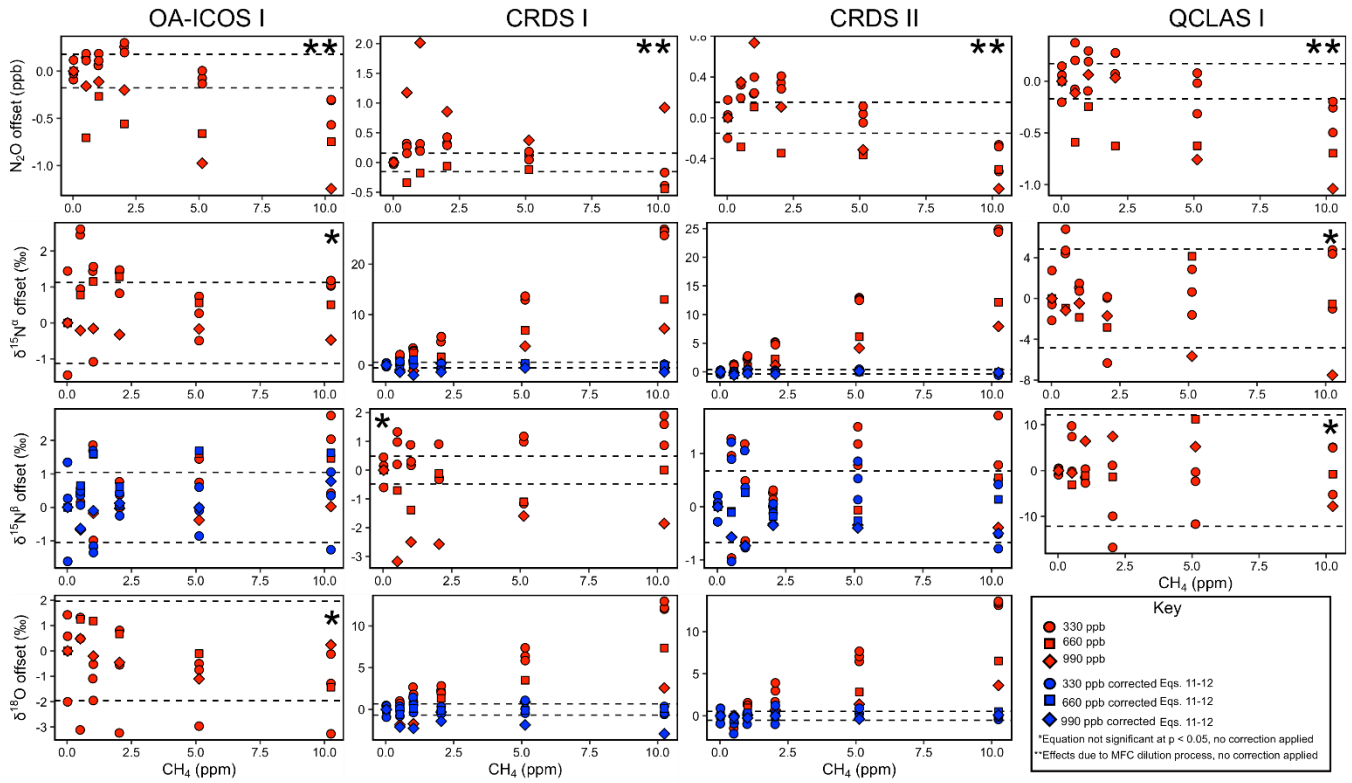

Fig. S6-3. Dependency of the measured N_2O mole fraction, $\delta^{15}N^{\alpha}$, $\delta^{15}N^{\beta}$ and $\delta^{18}O$ values on CH_4 (ppm) for OA-ICOS I, CRDS I, CRDS II, and QCLAS I. Non-corrected data is shown in red for various N_2O mole fractions tested (circle = 330 ppb; square = 660 ppb; diamond = 990 ppb). Corrected data using Eqs. (11-12) is shown in blue. The standard deviation of the Anchor gas (±1σ) is indicated by dashed lines.

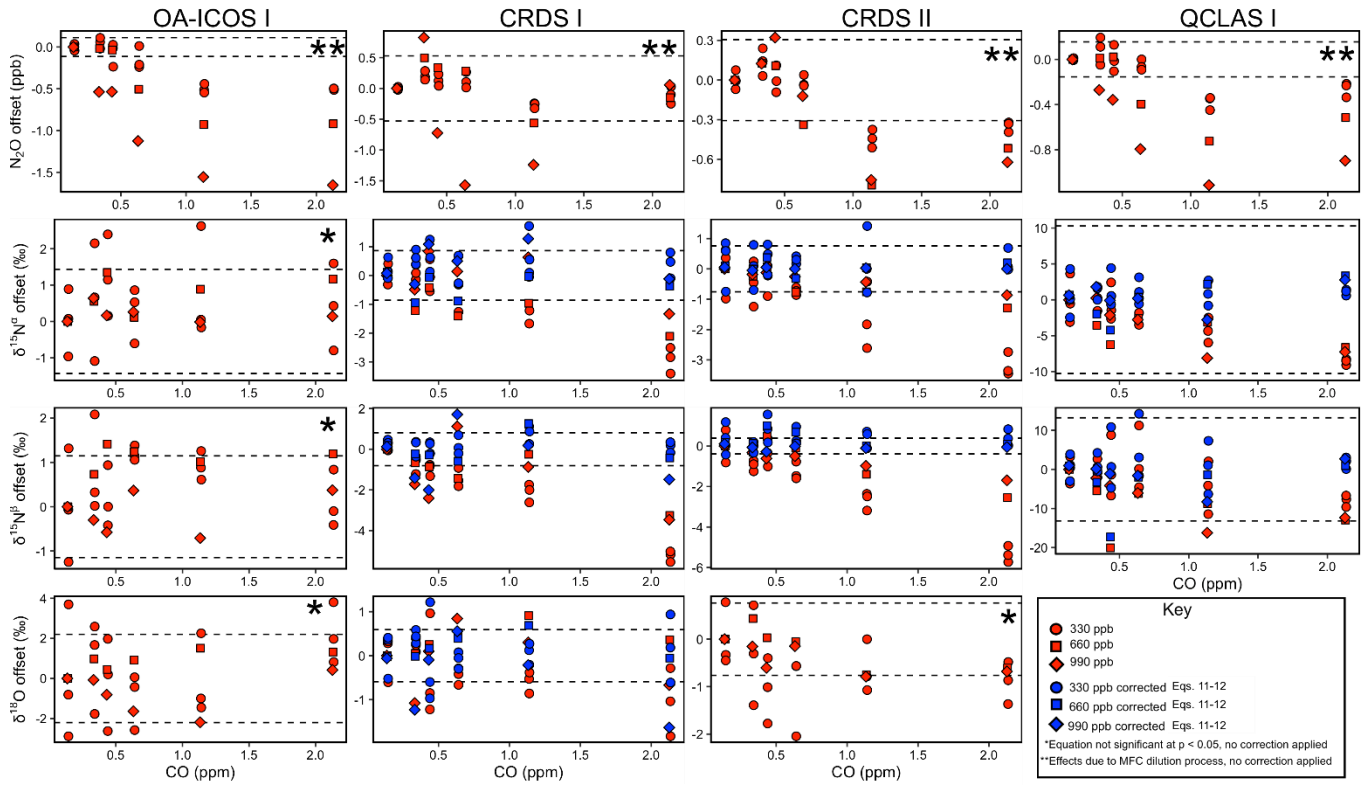

Fig. S6-4. Dependency of the measured N_2O mole fraction, $\delta^{15}N^{\alpha}$, $\delta^{15}N^{\beta}$ and $\delta^{18}O$ values on CO (ppm) for OA-ICOS I, CRDS I, CRDS II, and QCLAS I. Non-corrected data is shown in red for various N_2O mole fractions tested (circle = 330 ppb; square = 660 ppb; diamond = 990 ppb). Corrected data using Eqs. (11-12) is shown in blue. The standard deviation of the Anchor gas (±1σ) is indicated by dashed lines.

Table S6-1. The fitted constants A, B, and a, b and c for OA-ICOS I, CRDS I, CRDS II and QCLAS I, derived using Eqs. 5 and 6. For values of 0, there was either no apparent trend or the fitted values fell within the uncertainty of the measurements. The units for each constant are A: $1/(ppb_{N2O} \cdot \%_{O2})$, B: $1/\%_{O2}$, a: $‰/(ppb_{N2O}^2 \cdot \%_{O2})$, b: $‰/(ppb_{N2O} \cdot \%_{O2})$, and c: $‰/\%_{O2}$.

	N_2O [ppb]	$\delta^{15}N^{\alpha}$ [‰]	$\delta^{15}N^{\beta}$ [‰]	$\delta^{18}O$ [‰]
		OA-ICOS I		
A	$-5.97 \cdot 10^{-7}$	n.a.	n.a.	n.a.
a	n.a.	$-1.37 \cdot 10^{-8}$	$-2.57 \cdot 10^{-7}$	$-2.93 \cdot 10^{-6}$
B	$7.09 \cdot 10^{-5}$	n.a.	n.a.	n.a.
b	n.a.	$2.07 \cdot 10^{-4}$	$5.39 \cdot 10^{-4}$	$4.82 \cdot 10^{-3}$
c	n.a.	$1.00 \cdot 10^{0}$	$1.07 \cdot 10^{0}$	$-4.40 \cdot 10^{-1}$
		CRDS I		
A	$-2.40 \cdot 10^{-7}$	n.a.	n.a.	n.a.
a	n.a.	$7.74 \cdot 10^{-7}$	$7.71 \cdot 10^{-7}$	$7.55 \cdot 10^{-7}$
B	$8.67 \cdot 10^{-4}$	n.a.	n.a.	n.a.
b	n.a.	$-9.55 \cdot 10^{-4}$	$-4.71 \cdot 10^{-4}$	$-8.51 \cdot 10^{-4}$
c	n.a.	$-1.18 \cdot 10^{0}$	$-6.70 \cdot 10^{-1}$	$-4.40 \cdot 10^{-1}$
		CRDS II		
A	$-2.38 \cdot 10^{-7}$	n.a.	n.a.	n.a.
a	n.a.	$-3.11 \cdot 10^{-8}$	$-7.71 \cdot 10^{-8}$	$-8.34 \cdot 10^{-8}$
B	$1.08 \cdot 10^{-3}$	n.a.	n.a.	n.a.
b	n.a.	$6.71 \cdot 10^{-7}$	$1.93 \cdot 10^{-4}$	$2.03 \cdot 10^{-4}$
c	n.a.	$-9.09 \cdot 10^{-1}$	$-4.06 \cdot 10^{-1}$	$-3.92 \cdot 10^{-1}$
		QCLAS I		
A	$-2.20 \cdot 10^{-7}$	n.a.	n.a.	n.a.
a	n.a.	0	0	n.d.
B	$1.21 \cdot 10^{-3}$	n.a.	n.a.	n.a.

b	n.a.	0	0	n.d.
c	n.a.	0	0	n.d.

n.a. not applicable

n.d. not determined

Table S6-2. The fitted constants A_x, B_x, a_x and b_x, for OA-ICOS I, CRDS I, CRDS II and QCLAS I, derived using Eqs. 9 and 10. For values of 0, there was either no apparent trend or the fitted values fell within the uncertainty of the measurements. The unit for A_x and a_x is $ppm_{N2O}/ppm_{trace\ gas}$, and the unit for B_x and b_x is $1/ppm_{trace\ gas}$.

	$[N_2O]$		$\delta^{15}N^{\alpha}$		$\delta^{15}N^{\beta}$		$\delta^{18}O$	
	A	B	$a_{\delta 15N\alpha}$	$b_{\delta 15N\alpha}$	$a_{\delta 15N\beta}$	$b_{\delta 15N\beta}$	$a_{\delta 18O}$	$b_{\delta 18O}$
				OA-ICOS I				
CO_2	$-3.35\cdot10^{-4}$	$2.181\cdot10^{-3}$	$-1.50\cdot10^{-3}$	$-2.49\cdot10^{-3}$	$8.91\cdot10^{-3}$	$-1.86\cdot10^{-3}$	$-6.53\cdot10^{-3}$	$-6.25\cdot10^{-3}$
CH_4	0	0	0	0	$5.71\cdot10^{-2}$	0	0	0
CO	0	0	0	0	0	0	0	0
				CRDS I				
CO_2	$9.44\cdot10^{-5}$	$2.63\cdot10^{-4}$	$-7.780\cdot10^{-4}$	$-8.35\cdot10^{-4}$	0	0	$-1.32\cdot10^{-3}$	$-1.84\cdot10^{-3}$
CH_4	0	0	$8.42\cdot10^{-1}$	0	$2.651\cdot10^{-2}$	0	$3.99\cdot10^{-1}$	0
CO	0	0	$-4.05\cdot10^{-1}$	0	$-7.88\cdot10^{-1}$	0	$-1.34\cdot10^{-1}$	0
				CRDS II				
CO_2	$-5.04\cdot10^{-4}$	$2.07\cdot10^{-3}$	$3.20\cdot10^{-4}$	$2.30\cdot10^{-4}$	0	0	$-1.06\cdot10^{-3}$	$1.59\cdot10^{-3}$
CH_4	0	0	$7.94\cdot10^{-1}$	0	$3.71\cdot10^{-2}$	0	$4.27\cdot10^{-1}$	0
CO	0	0	$-4.66\cdot10^{-1}$	0	$-7.83\cdot10^{-1}$	0	$-2.03\cdot10^{-1}$	0
				QCLAS I				
CO_2	0	0	$-8.56\cdot10^{-6}$	0	$-5.73\cdot10^{-6}$	0	n.d.	n.d.
CH_4	0	0	0	0	0	0	n.d.	n.d.
CO	0	0	$-1.41\cdot10^{0}$	0	$-1.57\cdot10^{0}$	0	n.d.	n.d.

n.d. not determined

Supplementary Material 7 – Comparison with GC-IRMS

Fig. S7-1 shows the triplicate measurements (mean ± 1σ) obtained using the GC-IRMS plotted against expected mixing values calculated using MFC flow rates and the mole fraction and isotopic composition of *background* and *source*. A comparison between laser spectrometer and GC-IRMS measurements are presented in Figs. S7-2 to S7-5 using the mean ± 1σ of triplicate measurements. TREX-QCLAS I measurements were undertaken separately, and therefore were not directly compared to IRMS measurements.

There was excellent agreement between the IRMS and calculated expected isotope values (all $r^2 > 0.99$). Measurements for $\delta^{15}N^{\alpha}$, $\delta^{15}N^{\beta}$ and $\delta^{15}N^{bulk}$ were all typically within ± 1 ‰ of expected values, while SP was within ± 0.7 ‰ of expected values. $\delta^{18}O$ measurements were the poorest performing and were typically within ± 3 ‰ of expected values. The standard deviations of triplicate isotope measurements were typically between 0.1 – 1 ‰.

Generally, there is good agreement between the laser spectrometers and GC measurements, but disagreement between the two techniques becomes pronounced at higher ΔN_2O for OA-ICOS I and QCLAS I during experiments 5 and 6. All analyzers, with the exception of one triplicated measurement taken from CRDS I, showed better 1σ repeatability than those acquired using GC. There was excellent agreement for $\delta^{15}N^{\alpha}$, $\delta^{15}N^{\beta}$ and $\delta^{15}N^{bulk}$ between the IRMS and both CRDS I and II at all concentrations tested. $\delta^{15}N^{\alpha}$, $\delta^{15}N^{\beta}$ and $\delta^{15}N^{bulk}$ measurements for these analyzers were typically within ± 1 ‰ of those acquired from IRMS, while SP measurements were typically within ± 1.3 ‰. OA-ICOS I $\delta^{15}N^{\alpha}$, $\delta^{15}N^{\beta}$ and $\delta^{15}N^{bulk}$ measurements were typically within ± 2.5 ‰ of IRMS, while SP were in slightly better agreement (± 1.7 ‰). Conversely, QCLAS I showed good agreement with IRMS only at higher ΔN_2O (> 1,000 ppb), presumably due to less precise measurements that are expected (based on results acquired in Section 3) to be acquired at the lower concentrations tested. For OA-ICOS I, the repeatability of the triplicate $\delta^{15}N^{\alpha}$, $\delta^{15}N^{\beta}$, $\delta^{15}N^{bulk}$ and SP measurements was typically better than the IRMS exclusively at higher ΔN_2O (>1,000 ppb). CRDS I and II had comparable repeatability to the IRMS, and there was no

clear distinction based on ΔN_2O. QCLAS I showed comparable or better repeatability to IRMS only at higher ΔN_2O (>1,000 ppb).

$\delta^{18}O$ measurements from OA-ICOS I, and CRDS I and II showed good agreement with IRMS results (all $r^2 > 0.98$), with the vast majority of measurements similarly within ± 2‰. OA-ICOS I $\delta^{18}O$ measurements had typically better repeatability compared to IRMS at higher ΔN_2O, while both CRDS analyzers showed varied repeatability regardless of ΔN_2O.

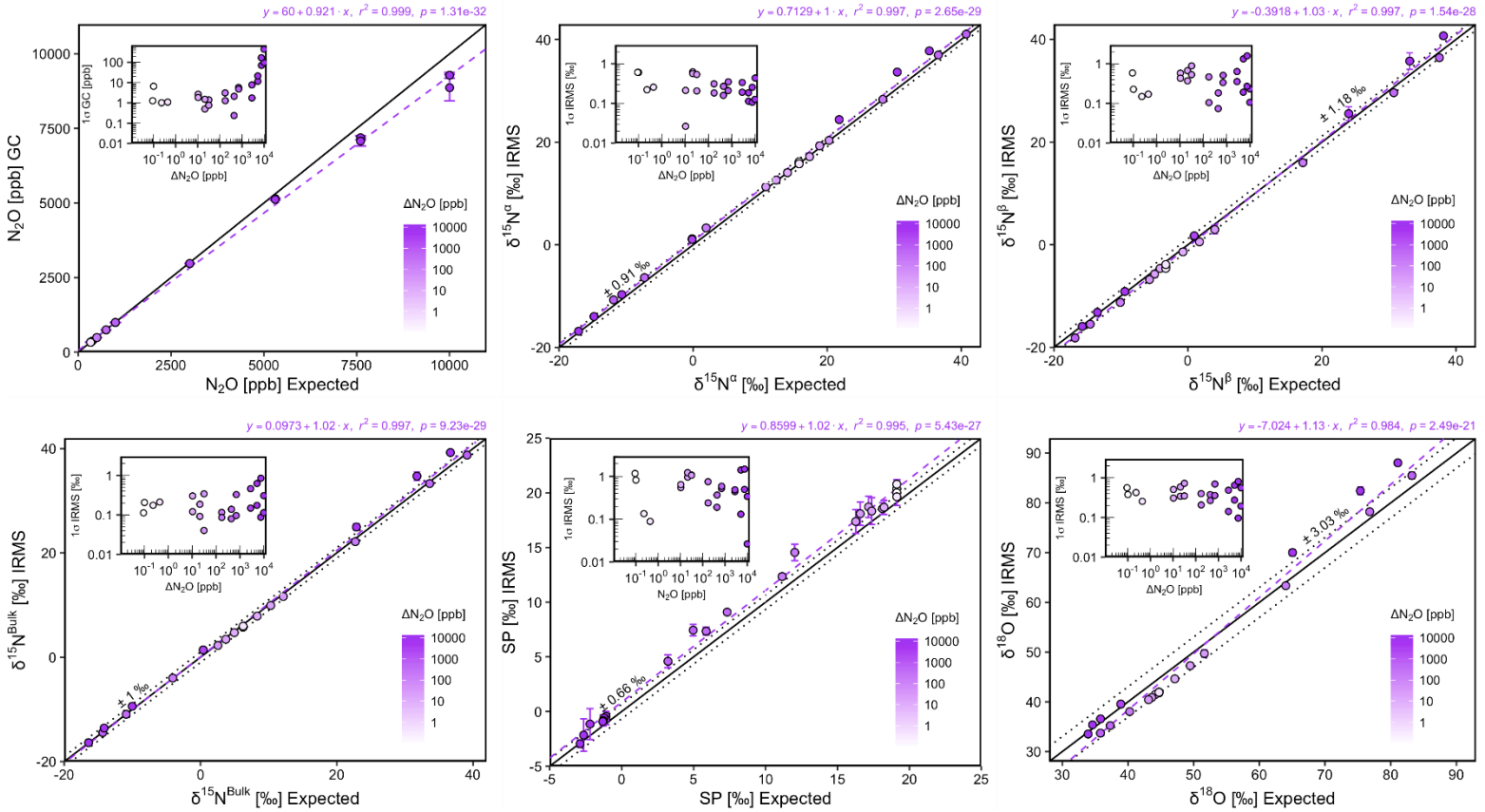

Fig. S7-1. Correlation diagrams for [N_2O], $\delta^{15}N^{\alpha}$, $\delta^{15}N^{\beta}$, $\delta^{15}N^{bulk}$, SP and $\delta^{18}O$ measurements at various ΔN_2O mole fractions analyzed by GC-IRMS plotted against expected values. The solid black line denotes the 1:1 line, while the dotted line indicates ±1σ of the residuals from the 1:1 line. The dashed black line represents a linear fit to the data. Individual equations, coefficients of determination (r^2) and p-values are indicated above each plot. Each data point represents the mean and standard deviation (1σ) of triplicate measurements. The inset plots indicate the standard deviation (1σ) of the triplicate measurements achieved at different ΔN_2O mole fractions, and the 1:1 line is similarly a solid line.

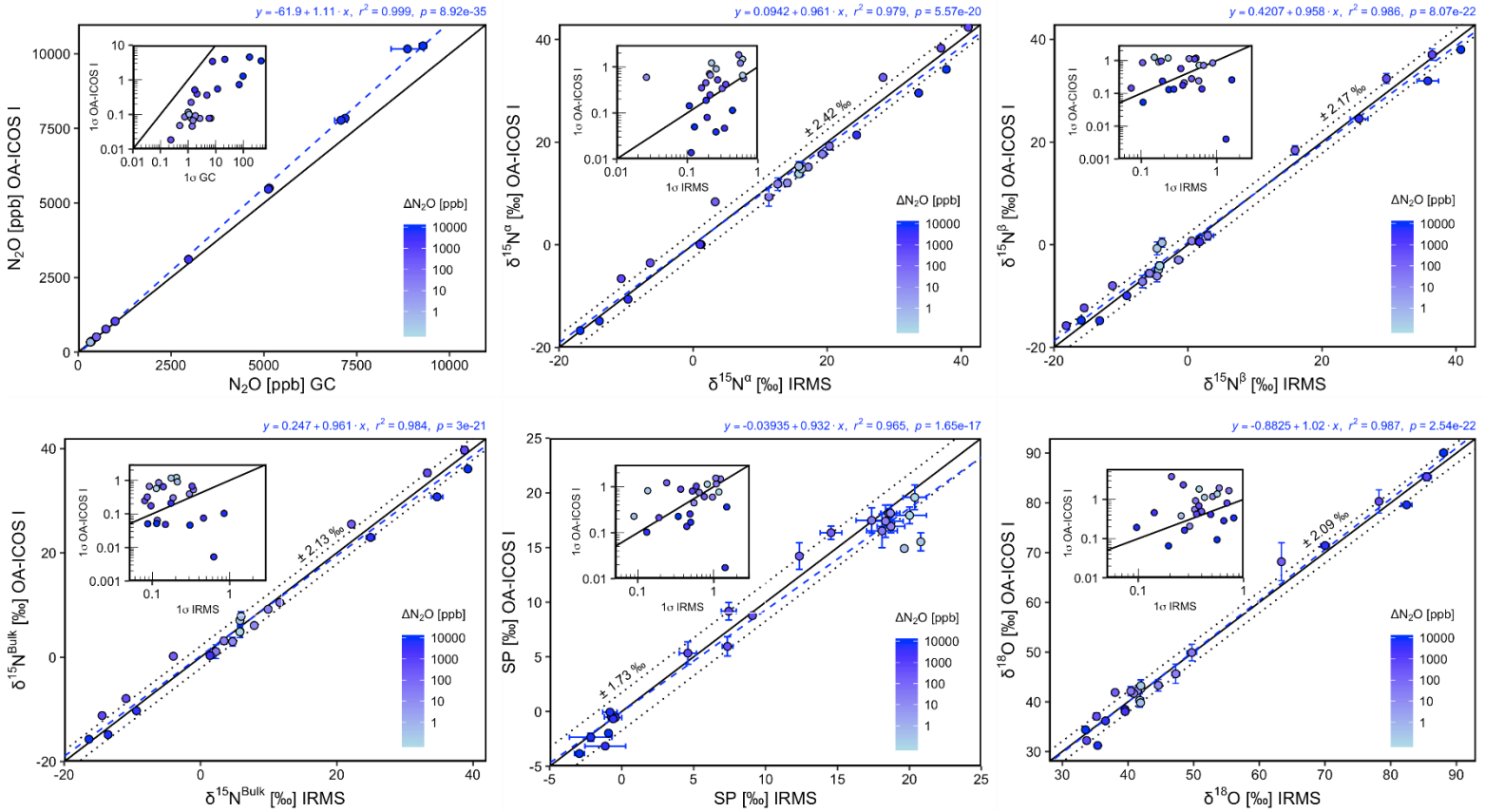

Fig. S7-2. Correlation diagrams for [N_2O], $\delta^{15}N^{\alpha}$, $\delta^{15}N^{\beta}$, $\delta^{15}N^{bulk}$, SP and $\delta^{18}O$ measurements at various ΔN_2O concentrations analyzed by both OA-ICOS I and GC-IRMS. The solid black line denotes the 1:1 line, while the dotted line indicates ±1σ of the residuals from the 1:1 line. The dashed blue line represents a linear fit to the data. Individual equations, coefficients of determination (r^2) and p-values are indicated above each plot. Each data point represents the mean and standard deviation (1σ) of triplicate measurements. The inset plots indicate the standard deviation (1σ) of the triplicate measurements achieved at different ΔN_2O concentrations, and the 1:1 line is similarly a solid line.

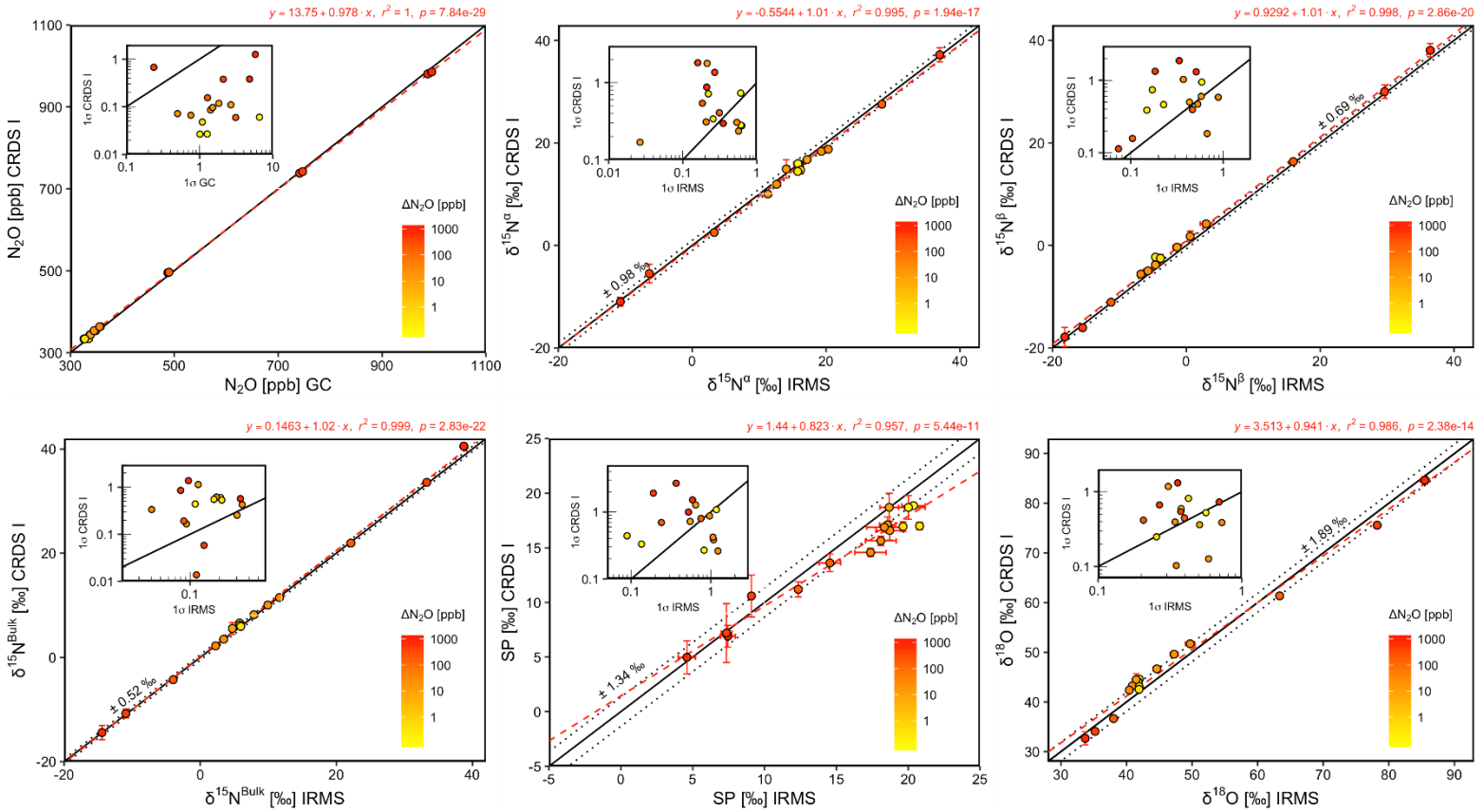

Fig. S7-3. Correlation diagrams for [N_2O], $\delta^{15}N^{\alpha}$, $\delta^{15}N^{\beta}$, $\delta^{15}N^{bulk}$, SP and $\delta^{18}O$ measurements at various ΔN_2O concentrations analyzed by both CRDS I and GC-IRMS. The solid black line denotes the 1:1 line, while the dotted line indicates ±1σ of the residuals from the 1:1 line. The dashed red line represents a linear fit to the data. Individual equations, coefficients of determination (r^2) and p-values are indicated above each plot. Each data point represents the mean and standard deviation (1σ) of triplicate measurements. The inset plots indicate the standard deviation (1σ) of the triplicate measurements achieved at different ΔN_2O concentrations, and the 1:1 line is similarly a solid line.

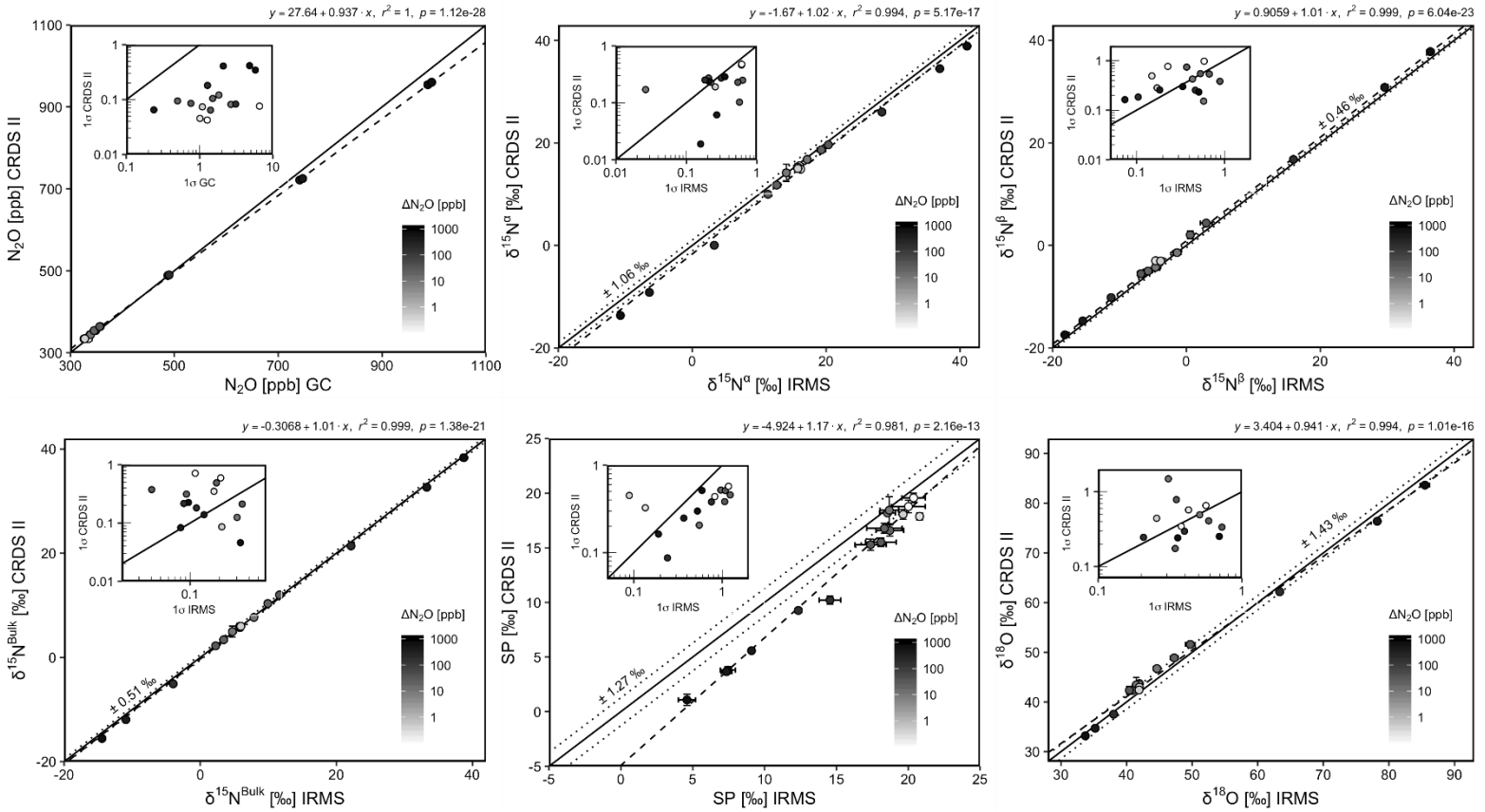

Fig. S7-4. Correlation diagrams for $[N_2O]$, $\delta^{15}N^{\alpha}$, $\delta^{15}N^{\beta}$, $\delta^{15}N^{bulk}$, SP and $\delta^{18}O$ measurements at various ΔN_2O concentrations analyzed by both CRDS II and GC-IRMS. The solid black line denotes the 1:1 line, while the dotted line indicates ±1σ of the residuals from the 1:1 line. The dashed black line represents a linear fit to the data. Individual equations, coefficients of determination (r^2) and p-values are indicated above each plot. Each data point represents the mean and standard deviation (1σ) of triplicate measurements. The inset plots indicate the standard deviation (1σ) of the triplicate measurements achieved at different ΔN_2O concentrations, and the 1:1 line is similarly a solid line.

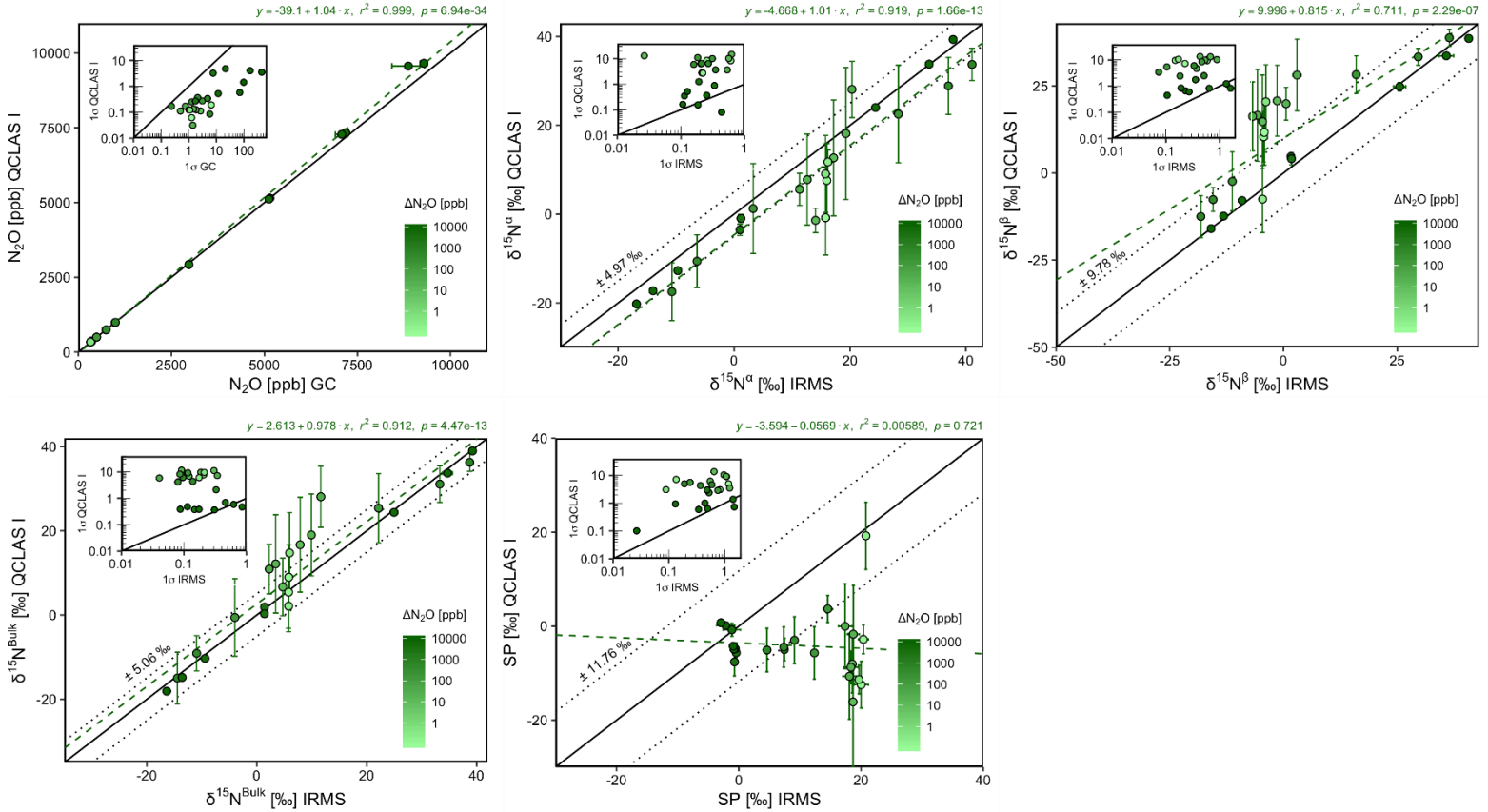

Fig. S7-5. Correlation diagrams for [N_2O], $\delta^{15}N^{\alpha}$, $\delta^{15}N^{\beta}$, $\delta^{15}N^{bulk}$ and SP measurements at various ΔN_2O concentrations analyzed by both QCLAS I and GC-IRMS. The solid black line denotes the 1:1 line, while the dotted line indicates ±1σ of the residuals from the 1:1 line. The dashed green line represents a linear fit to the data. Individual equations, coefficients of determination (r^2) and p-values are indicated above each plot. Each data point represents the mean and standard deviation (1σ) of triplicate measurements. The inset plots indicate the standard deviation (1σ) of the triplicate measurements achieved at different ΔN_2O concentrations, and the 1:1 line is similarly a solid line.